Arrhythmogenic Transient Dynamics in Cardiac Myocytes

Yuanfang Xie, Leighton T. Izu, Donald M. Bers, and Daisuke Sato*
Departments of Pharmacology, University of California Davis, Davis, California

ABSTRACT Cardiac action potential alternans and early afterdepolarizations (EADs) are linked to cardiac arrhythmias. Periodic action potentials (period 1) in healthy conditions bifurcate to other states such as period 2 or chaos when alternans or EADs occur in pathological conditions. The mechanisms of alternans and EADs have been extensively studied under steady-state conditions, but lethal arrhythmias often occur during the transition between steady states. Why arrhythmias tend to develop during the transition is unclear. We used low-dimensional mathematical models to analyze dynamical mechanisms of transient alternans and EADs. We show that depending on the route from one state to another, action potential alternans and EADs may occur during the transition between two periodic steady states. The route taken depends on the time course of external perturbations or intrinsic signaling, such as β-adrenergic stimulation, which regulate cardiac calcium and potassium currents with differential kinetics.

INTRODUCTION

Cardiac arrhythmia is the leading cause of sudden cardiac death (1). Under normal conditions, cardiac action potentials (APs) are periodic (period 1). Under pathological conditions, the periodic APs bifurcate to alternans or early afterdepolarizations (EADs), which are dynamically linked to period 2 (2) and chaos (3,4). As precursors to life-threatening arrhythmias, both AP duration (APD) alternans and EADs can be induced by voltage- or calcium (Ca)-driven instability. Whereas Ca-driven alternans and EADs are determined by the instability of intracellular Ca cycling, voltage-driven alternans and EADs are often associated with deficiencies in potassium (K) currents or enhancements in the Ca or sodium current (such as in long-QT syndrome types 1–3 and 8) (5–8).

The underlying dynamical and ionic mechanisms of APD alternans and EADs have been extensively investigated at steady states (3,4,9–11). Lethal arrhythmias, however, are often observed during transitions rather than steady states (6,12–14). These transient arrhythmias are commonly related to β-adrenergic signaling, which regulates cardiac ion channels with differential kinetics (15–18). Isoproterenol (ISO), a β-adrenergic agonist, activates the L-type Ca current (I_{CaL}) more quickly than the slow delayed rectifier potassium current (I_{Ks}) (13). In line with this, ISO application was found to transiently prolong APD in normal cardiac cells (13,19–21) and induce EADs transiently in pathological conditions (13). ISO stimulation also leads to episodes of T-wave alternans (12) which are caused by APD alternans at fast pacing rate. These transient phenomena, referred to as biological adaptation or compensation (22,23), are often overlooked, and their connection to cardiac arrhythmias rarely has been made.

In our previous study, using a physiological detailed model (24), we investigated ionic mechanisms by which all the targets of β-adrenergic stimulation affect transient EADs. Here, we aim at the dynamical mechanisms of transient APD alternans and EADs using a simplified ionic-current model of ISO application to understand how cardiac myocytes may transiently exhibit these arrhythmogenic phenomena in a generic way. With the simplified model, we were able to take advantage of the differential timescales of I_{Ks} and I_{CaL} activation by ISO stimulation to reduce the high-dimensional system to its most fundamental properties during the AP plateau phase so that we could focus on the underlying dynamical mechanisms of transient APD alternans and EADs.

METHODS

To elucidate the generic mechanisms, we used two simplified three-variable AP models that capture the instability around the plateau membrane voltage. The governing equation of the models is $dV/dt = (-I_m + I_{sti})/C_m$, where V is the membrane voltage, C_m is the membrane capacitance, I_m refers to the transmembrane currents, and I_{sti} is the stimulation. We used the three-current model $(I_m = I_{Na} + I_{Ca} + I_K)$ (25,26) to investigate alternans. The state variables of this model are V, inactivation gate of I_{Na} (h), and inactivation gate of I_{Ca} (f). The two-current model $(I_m = I_{Ca} + I_K)$ (3) was used to investigate EADs. This model consists of variables V, f, and the activation gate of I_K (x).

Two transient routes are introduced by different protocols of ISO application, sudden and gradual. In sudden application, ISO is instantaneously switched from 0 to 100% at time 0 (Fig. 1 *a*, *upper*). In gradual application, ISO is applied in a stepwise manner used in experiments (27) (Fig. 1 *b*, *upper*), at 20% per step, reaching the same amount of ISO as in the case of sudden application. Both models respond to ISO stimulation by changing the maximum conductance of I_{Ca} (G_{Ca}) and I_K (G_K) over time (i.e., $G(t)$). $G(t)$ is fitted with a single-exponential function, $G(t) = G_0 + G_{ISO}(1 - \exp(-t/\tau))$, where G_0 is the G_{Ca} or G_K before ISO application, G_{ISO} is the increment induced by ISO, and τ is the time constant of ISO activation, as shown in experiments (13). τ_{GCa} is eight times faster than τ_{GK}(see figure legends). This difference between τ_{GCa} and τ_{GK} is on the same order as the experimental data (13). The dose effect of ISO in gradual application was

Submitted July 15, 2013, and accepted for publication December 31, 2013.

*Correspondence: dsato@ucdavis.edu

Editor: Peter Hunter.

0006-3495/14/03/1391/7 $2.00

http://dx.doi.org/10.1016/j.bpj.2013.12.050

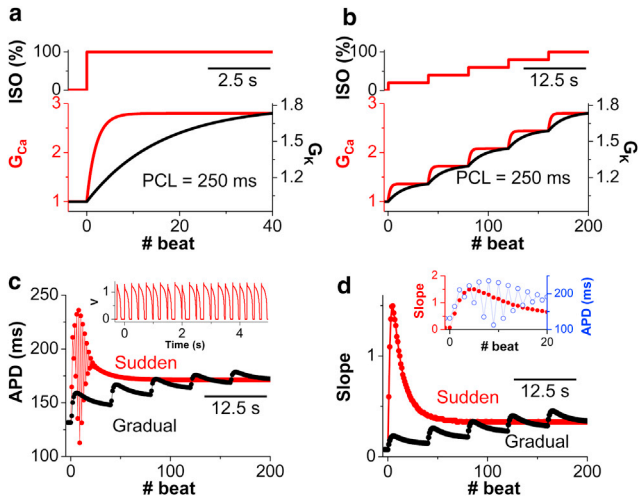

FIGURE 1 Transient APD alternans is induced by sudden, but not by gradual, application of ISO. (*a* and *b*) Protocol of ISO application and its effect on G_{Ca} (*red*) and G_K (*black*) in sudden (*a*) and gradual (*b*) application. $\tau_{GCa} = 500$ ms and $\tau_{GK} = 4000$ ms. (*c* and *d*) APD traces and slope of APD restitution in sudden (*red*) and gradual (*black*) application of ISO at PCL 250 ms. (*Insets*) Voltage trace (*c*) and slope with its corresponding APD (*d*) in the case of sudden application of ISO. To see this figure in color, go online.

linearly interpolated (Fig. 1 *b*, *lower*). No alternans or EADs occur at either steady state before or after ISO application.

RESULTS

Transient alternans by the sudden application of ISO

Transient APD alternans occurs when ISO is applied suddenly (Fig. 1 *c*, *red*), but not when it is applied gradually (Fig. 1 *c*, *black*). In the case of sudden application, APD prolongs rapidly due to the faster increase of I_{Ca} versus I_K (Fig. 1 *a*). This APD prolongation shortens the following diastolic interval (DI) for the first two beats (Fig. 1 *c*, *inset*). When DI is too short for the recovery of I_{Ca} at the third beat, APD decreases and leads to a slightly longer DI which is followed by a longer APD (fourth beat). Consequently, APD alternans develops. As G_{Ca} approaches its steady state, G_K continues to increase, which shortens the APD. As a result, the DI increases and APD alternans decreases. Eventually, APD alternans disappears when the increase of I_K counteracts I_{Ca}.

Inhibition of I_{Ca} (or enhancement of I_K) is shown to be antiarrhythmic by flattening the APD restitution (28–30); ISO stimulation (31) or β-adrenergic receptor antagonists (32) are reported to steepen or flatten, respectively, the APD restitution. These alter the APD restitution steepness by changing the relative contribution of I_{Ca} to the APD restitution, since I_{Ca} determines its steepness (28,30). A quick increase of I_{Ca} versus I_K by sudden ISO application can also steepen the APD restitution transiently and lead to transient APD alternans. We calculated the slope of the APD restitution curve at fixed points (using the control method of alternans for unstable fixed points (33–35) and the perturbation method for stable ones) during ISO application. Due to the lack of memory and Ca cycling in this simplified model, APD is only a function of the previous DI. Thus, APD alternans develops when the slope of the restitution curve exceeds unity (36,37). In the case of sudden application (Fig. 1 *d*, *red*), at the second beat after ISO application, the APD restitution slope exceeds unity, where APD alternans starts to occur (Fig. 1 *d*, *inset*). The amplitude of APD alternans keeps growing when the slope is >1 (until the 10th beat after ISO application) and then decreases when the slope is <1 as I_K activation starts catching up. In the gradual application, however, the slope is always <1 (Fig. 1 *d*, *black*).

Fig. 2 *a* shows the maximal cycle length (CL) at which APD alternans can be seen (coded by color) in the G_{Ca}-G_K parameter space. As G_{Ca} is increased and/or G_K is decreased, APD alternans develop at slower pacing rates. In other words, the system becomes more unstable with larger G_{Ca} and/or smaller G_K. At the steady state before and after ISO application, the system stays at points labeled 1 and 3, respectively, in the G_{Ca}-G_K parameter space. No alternans occurs at these states (Fig. 2 *b*, *black and blue dots*). The route from point 1 to point 3 depends on the protocol of ISO application. The red and blue arrows in Fig. 2 *a* trace changes of (G_K, G_{Ca}) during the rapid and gradual ISO applications shown in Fig. 1, *a* and *b*, respectively. The black dotted line indicates the stable limit in the G_{Ca}-G_K space for the pacing cycle length (PCL) of 250 ms used in Fig. 1. The system is stable below this line and unstable above it. When ISO is applied rapidly, the (G_K, G_{Ca}) path crosses the stable limit and alternans develops (Fig. 2 *B*, *red dots*). Under gradual ISO application, however, all (G_K, G_{Ca}) points on the path marked by the blue arrows are stable, and no alternans develops. Note also that steady-state alternans can also be seen for both control and ISO conditions at shorter CLs (bifurcations in black and blue curves in Fig. 2 *b*).

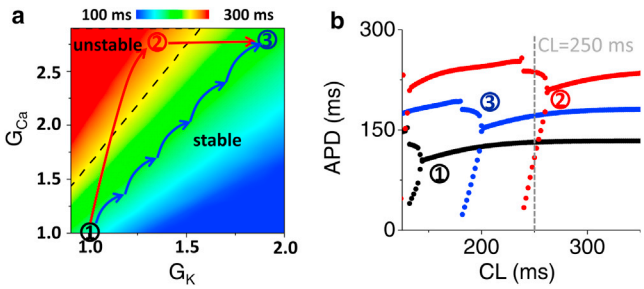

FIGURE 2 (*a*) Diagram of APD alternans onset in the G_{Ca}-G_K parameter space. Three states were mapped in the diagram: the steady states before (1) and after (3) ISO application and the transient state at the eighth beat after sudden ISO application (2). Red and blue arrows indicate the routes of sudden and gradual application, respectively, as in Fig. 1. The dotted line is the PCL used in Fig. 1 *b*. (*b*) Bifurcation of APD before ISO (1, *black*), after ISO (3, *blue*), and in the transient state (2, *red*) shown in *a*. To see this figure in color, go online.

Similar results are observed with a physiologically detailed model by Mahajan et al. (38) in regimes where APD alternans is voltage-driven (Fig. S2 in the Supporting Material), although it should be noted that alterations in Ca handling can also lead to alternans in this regime (38).

Transient EADs induced by the sudden application of ISO

In addition to APD alternans, this transient mismatch between I_{Ca} and I_K upon the sudden application of ISO also induces transient EADs when APDs are significantly prolonged (Fig. 3 *a* , *inset*, *red stars*). In the gradual application of ISO (Fig. 3 *b*), however, the APD increases more modestly (only during the first two beats) and then shortens without EADs.

To understand how sudden application of ISO tends to generate transient EADs, we first investigate the necessary conditions for EAD generation in our minimal model (Eq 1).

$$C_m\frac{dV}{dt} = -G_{Ca}d_\infty f(V-E_{Ca}) + G_K x(V-E_K) \tag{1a}$$

$$\frac{df}{dt} = \frac{f_\infty - f}{\tau_f} \tag{1b}$$

$$\frac{dx}{dt} = \frac{x_\infty - x}{\tau_x}, \tag{1c}$$

where d_∞ is the steady state of the fast activation gate of I_{Ca} (whose time constant is <5 ms (39)); f_∞ and x_∞ are the steady states of f and x, respectively, with time constants τ_f and τ_x; $C_m = 1$ pF/pA; $V = V(t)$, $f = f(t)$; and $x = x(t)$. Reversal potentials of I_{Ca} and I_K are set as $E_{Ca} = 100$ mV and $E_K = -80$ mV, respectively. The AP is initiated by a delta function that brings the voltage from the resting potential to 0 mV upon pacing.

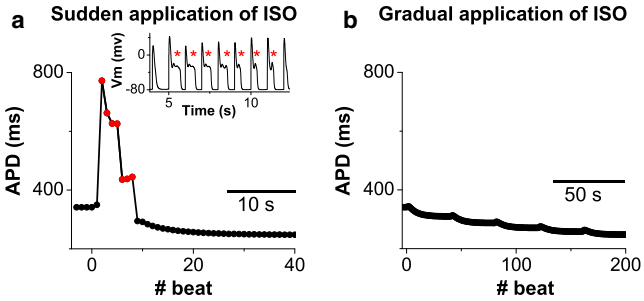

FIGURE 3 Transient EADs are induced by sudden (*a*), but not by gradual (*b*), application of ISO. The protocol of ISO application is the same as in Fig. 1. Red dots in *a* indicate EADs (see *inset*). $\tau_{GCa} = 1000$ ms; $\tau_{GK} = 8000$ ms; PCL = 1000 ms. To see this figure in color, go online.

$$G(V,f) = \frac{f_\infty - f}{\tau_f}. \tag{2b}$$

Fixed points of the subsystem (V,f) can be visualized in *I/V* plots (Fig. 4 *a*). At steady state, $-I_{Ca} = -G_{Ca}d_\infty f_\infty(V-E_{Ca})$ is a bell-shaped window current (*red line*) and $G_K x(V-E_K)$ is linear (*blue solid line*), with its slope increasing with x (*blue dotted line*) The intersections of I_{Ca} and I_K are fixed points (FPs), as the net current is zero. When x is small, three fixed points (Fig. 4 *a*, *green dots*)—the resting state (FP_1), the excitation threshold (FP_2), and the excited state (FP_3)—coexist, forming bistability of voltage. As x increases, bistability disappears (*blue dashed line*, where FP_2 and FP_3 merge). The black dotted line in Fig. 4 *a* indicates the bifurcation point (i.e., the critical *V*, V_c). V_p is defined as the voltage for the peak window I_{Ca}. FP_3, with its voltage above V_p, has a negative conductance, which can form (damped) oscillations in the (V,f) space. Since EADs are voltage oscillations at the AP plateau, we analyze stability of FP_3 in the (V,f) subsystem for conditions of EADs.

The stability of FP_3 is calculated using the eigenvalue of the Jacobian matrix (Eq. 3) of Eq. 2.

$$\begin{bmatrix} F_V & F_f \\ G_V & G_f \end{bmatrix} = \begin{bmatrix} -G_{Ca}d'_\infty f(V-E_{Ca}) - G_{Ca}d_\infty f - G_K x & -G_{Ca}d_\infty(V-E_{Ca}) \\ \dfrac{f'_\infty}{\tau_f} & \dfrac{-1}{\tau_f} \end{bmatrix}. \tag{3}$$

Fast-slow subsystem analysis

Since x is much slower than V and f (τ_x is on the order of several hundred milliseconds (40)), we further reduce the three-variable system (Eq. 1) to the fast two-variable subsystem (V,f) (Eq. 2), and the slow variable x ($x \in [0,1]$) is treated as a parameter (fast-slow subsystem analysis (41)).

$$F(V,f) = -G_{Ca}d_\infty f(V-E_{Ca}) + G_K x(V-E_K) \tag{2a}$$

The eigenvalues of Eq. 3. are $\lambda_{1,2} = (tr \pm \sqrt{\Delta})/2$, where tr is the trace and Δ is the determinant linearized about FP_3. Fig. 4 *b* shows the sign of Δ and tr of FP_3 at $x = 0.1$ (Similar patterns occur for $x \in [0,1]$) in the (V,τ_f) parameter space.) If V and τ_f are within the blue area ($\Delta < 0$, $tr < 0$), damped oscillation occurs. If V and τ_f are within the red area ($tr > 0$), FP_3 is unstable. It is noteworthy that $\Delta > 0$ (*red area*) occurs at lower voltage than $\Delta < 0$ (*blue area*), regardless of τ_f. This means that

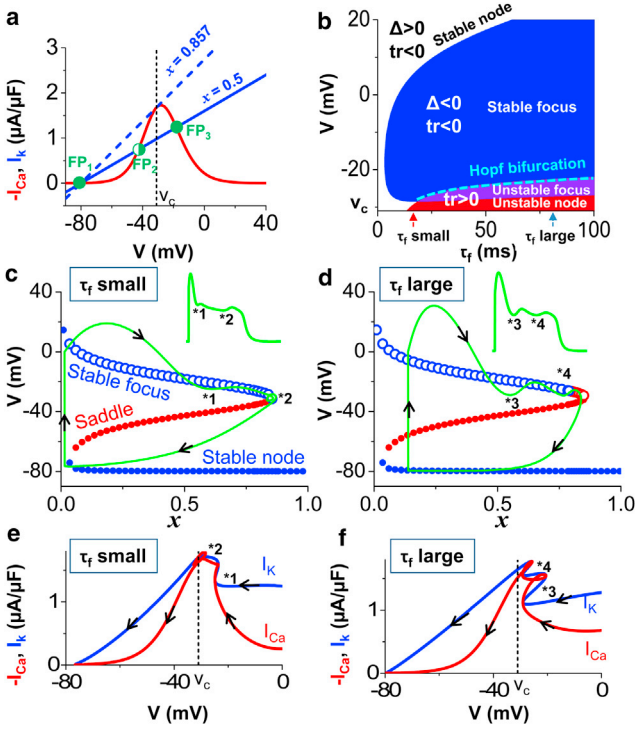

FIGURE 4 Dynamical mechanism of EADs. (*a*) Steady-state *I/V* curve plots of I_{Ca} (*red*) and I_K (*blue*). The black dotted line (V_c) indicates the bifurcation for bistability. Green dots are fixed points. (*b*) Eigenvalue analysis of FP_3 in the (V,τ_f) parameter space. The purple area (intersection of red ($tr>0$) and blue areas ($\Delta<0$)) indicates the Hopf bifurcation (*cyan dashed line*). Red (small τ_f) and blue (large τ_f) arrows mark two bifurcation scenarios shown in c and *d*. (*c* and *d*) Mechanism of EAD illustrated by the fast ((V,f))-slow (x) subsystem analysis at small (τ_f =18 ms) and large τ_f (τ_f =80 ms), respectively, showing stable-focus FP_3 (*blue circles*) and unstable-focus FP_3 (*red circles*). (*Inset*) The voltage trace (*green line*) is mapped into the *V-x* plane, and its time course is indicated (*black arrows*). τ_x =100 ms (*c*) and 300 ms (*d*). (*e* and *f*) *I/V* plots corresponding to the AP plateaus in *c* and *d*, respectively, indicating the existence of bistability for EADs. Numbers 1–4 labeled with asterisks indicate the reversal points of voltage for EADs. To see this figure in color, go online.

FP_3 at high voltage, away from V_c, is a stable focus (Fig. 4, *c* and *d*, *blue open circles*). The purple area (overlap of the red ($tr > 0$) and blue areas ($\Delta < 0$) in Fig. 4 *b*) represents the unstable focus, which only exists at relatively large τ_f, and close to V_c (Fig. 4 *d*, *red circles*). Thus, the Hopf bifurcation points (Fig. 4 *b*, *cyan dashed line*, where $tr = 0$ and $\Delta < 0$) only exist when τ_f is not small. Therefore, depending on τ_f, there are two scenarios for voltage oscillations. If τ_f is small (e.g., Fig. 4 *b*, *red arrow*), FP_3 is always stable (Fig. 4 *c*), such that only damped voltage oscillations can occur. On the other hand, if τ_f is large (e.g., Fig. 4 *b*, *blue arrow*), FP_3 changes from stable focus to unstable focus through the Hopf bifurcation as V approaches V_p (Fig. 4 *d*), such that voltage oscillations with increasing amplitude can occur after Hopf bifurcations.

Two necessary conditions for EAD generation

The stability analysis shown above provides the necessary conditions for EAD generation. The first necessary condition is the existence of FP_3, in other words, the bistability in the (V,f) subsystem. Oscillations of the membrane voltage (i.e., EADs) occur around this FP. Fig. 4, *e* and *f*, shows I_{Ca} (*red*) and I_K (*blue*) during the plateau of the AP shown in the insets of Fig. 4, *c* and d, respectively. As the repolarization proceeds (*arrows*) toward V_c (*dotted line*), I_K hits the quasiwindow I_{Ca} (Fig. 4, *c* and *d*, **1*, **2*, **3*, and **4*), reversing the voltage and forming EADs.

In the whole system (*V-f-x*), x increases slowly. At the same time, the size of the basin of attraction for FP_3 in the (V,f) subsystem decreases (Fig. 5 *a* , *red area*). x is small at the beginning of the AP plateau; thus, FP_3 in the subsystem (V,f) is a stable focus (Fig. 4 *b*). To generate EADs, the system must be trapped by this attractor. Therefore, a large basin of attraction for the stable-focus FP_3 (to attract the voltage spiral toward it) in the (V,f) subsystem is the second condition for EAD generation.

Since two different bifurcations of FP_3 exist in the (V,f) subsystem, depending on τ_f (Fig. 4 *b*), we illustrate the formation of EADs in both situations by projecting the AP to the *V-x* space. When τ_f is small (Fig. 4 *c*, $\tau_f = 18$ ms (Fig. 4 *b*, *red arrow*)), FP_3 is stable at all x values (Fig. 4, *c* and *d*, *upper branch*, *blue circles*). The membrane voltage

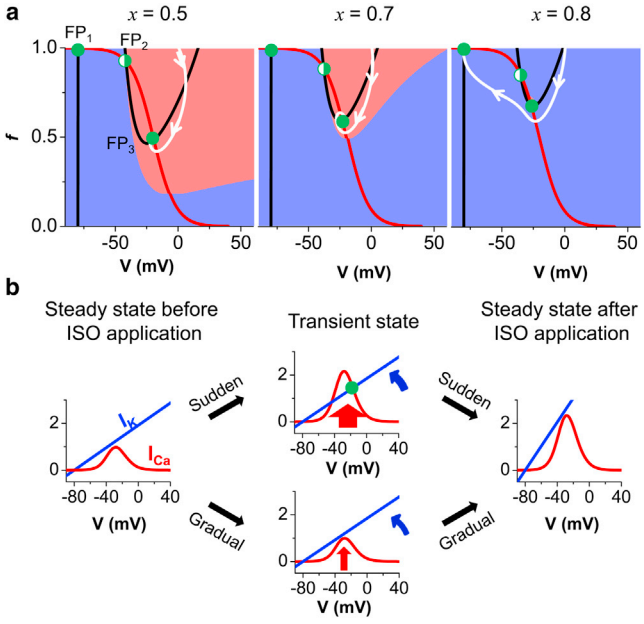

FIGURE 5 Mechanism of transient EADs induced by sudden ISO application. (*a*) Basin of attraction for FP_3 (*red*) decreases as x increases. Fixed point (*green dot*) is the intersection of *V* nullcline (*black line*) and *f* nullcline (*red line*). Plateau voltage (*white line and arrows*) evolves toward (at small x) or bypasses (at large x) FP_3. (*B*) Schematic plot shows evolution route of *I/V* plots of I_{Ca} and I_K in sudden (*upper*) and gradual (*lower*) ISO application. Green dot represents FP_3. To see this figure in color, go online.

(*green curve*) spirals toward the stable focus (*arrows*) and then exits through the saddle node bifurcation, giving rise to EADs. The two reversal points of V (*1 and *2) in the *V-x* plane correspond to the notch (Fig. 4 *c*, *inset*, **1*) and EAD (Fig. 4 *c*, *inset*, **2*), respectively. When τ_f is relatively large (Fig. 4 *d*, $\tau_f = 80$ ms, blue arrow in Fig. 4 *b*), FP_3 becomes unstable (Fig. 4, *c* and *d*, *red circles*) at large x (associated with a voltage approaching V_c) through supercritical Hopf bifurcation. In a similar way, EADs develop (Fig. 4 *d*, **3* and **4*) by spiraling toward the stable focus at first, but they then end through Hopf-homoclinic bifurcation (4) if x is slow enough. In both cases, the two necessary conditions for EAD generation are satisfied.

The mechanism of transient EADs induced by the sudden application of ISO

How does the modulation of I_{Ca} and I_K by ISO affect EAD generation? The sudden application of ISO (Fig. 5 *b*, *upper route*) causes a much larger increase of I_{Ca} (*red*) compared to I_K (*blue*) transiently, which favors the two conditions of EAD generation. First, it enhances the propensity toward bistability in the (V,f) subsystem (intersection marked by the green dot in Fig. 5 *b*). Second, it increases the basin of attraction for the stable focus at plateau V (which shrinks as x increases, Fig. 5 *a*) in the (V,f) subsystem, thereby potentiating the plateau voltage to spiral into its basin. On the other hand, in the adequately gradual application of ISO (Fig. 5 *b*, *lower route*), the increase of I_{Ca} is always compensated by the increase in I_K, resulting in little effect on the generation of bistability and the size of the basin of attraction. Thus, EADs are less likely to occur.

In the whole system, phase plots illustrate these different effects of ISO on EAD generation by projecting APs into the *x-f* plane (Fig. 6). Despite the protocols of application, the same period 1 attractor exists for both cases after ISO application (Fig. 6, *red*). In the sudden application (Fig. 6, *left*), the system evolves away (Fig. 6, *black*) from the initial periodic steady state (Fig. 6, *green*) and into the irregular EADs transiently due to the large increase of I_{Ca} versus I_K caused by application of ISO. As the increase in I_K counteracts the effects of I_{Ca}, the system evolves back to the new periodic steady state (Fig. 6, *red*). In the gradual application (Fig. 6, *right*), however, the increase of I_K always matches that of I_{Ca}, so that the emerging attractor is always close to the old one. Thus, the system evolves gradually between two periodic attractors along semi-steady states and no EAD occurs.

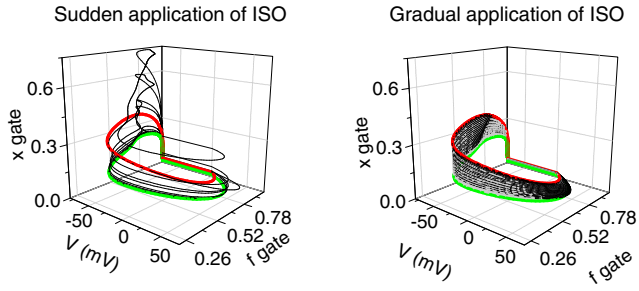

FIGURE 6 Attractors and trajectories in the phase space in sudden (*left*) and gradual (*right*) ISO application of Fig. 3. Green and red curves are the steady-state APs before and after ISO application, respectively. Black curves represent the transient states. To see this figure in color, go online.

DISCUSSION

In this study, we show that cardiac cells can have different transient behaviors depending on the protocol of βAR stimulation. Sudden, but not gradual, activation of βAR (by ISO) promotes transient APD alternans and EADs. In addition, sudden application of ISO promotes transient Ca alternans.

Transient behavior is common in both physiological and pathological conditions in biological systems (12,42,43). However, most prior studies on cardiac arrhythmias have focused on the steady state and ignored the dynamics during the transient process (7,8,11,18,44). Our work shows that arrhythmogenic APD alternans and EADs can occur during the transition between stable steady states from the dynamical point of view. Assessment of antiarrhythmic drug efficacy could be wrong if the transient dynamics are ignored. A drug that is antiarrhythmic at steady state may be proarrhythmic during the transition.

In addition, our study shows that a stable limit cycle in the fast (V,f) subsystem is not required for EAD generation (Fig. 4, *c* and *d*). The two necessary conditions for EAD generation are 1), the existence of stable focus at the plateau voltage in the (V,f) fast subsystem, which can be approximated by bistability in the *I*/*V* plot of I_K and window I_{Ca}; and 2), the ability of these stable foci to attract the plateau membrane voltage.

Although many currents contribute to voltage-instability-driven APD alternans, I_{CaL} is the major current that steepens the APD restitution (28) and can be modulated by ISO stimulation (31). Therefore, a sudden ISO stimulation can be arrhythmogenic by causing APD alternans, EADs, or both through the same ionic mechanisms (i.e., fast increase of I_{CaL} versus I_{Ks}). The minimal model allows us to capture the essential dynamical features of transient APD alternans (Fig. S2) and EADs (24), which are generic and valid for physiological detailed models.

Instability of the intracellular Ca is also very important for APD alternans. Alternans can be induced by steep APD restitution, a steep relationship between the Ca release from the sarcoplasmic reticulum (SR) and the SR Ca load, or both. Increase of I_{CaL} leads to Ca overload, which promotes Ca alternans. On the other hand, increase of the sarcoendoplasmic reticulum calcium transport ATPase (SERCA) pump activity suppresses alternans (45).

When ISO is applied suddenly, I_{CaL} is activated, and this promotes Ca alternans. Then, as SERCA is activated, Ca alternans disappears (Fig. S4). Similar to the case of APD

alternans, gradual application of ISO does not induce Ca alternans (data not shown). In this case, transient Ca alternans occurs due to the differential kinetics of activation of I_{CaL} and SERCA by ISO stimulation. Membrane voltage and intracellular Ca cycling are coupled via Ca-sensitive currents such as I_{CaL} and Na-Ca exchange. A larger Ca transient can prolong the APD through the sodium-calcium exchanger. On the other hand, the larger Ca transient can shorten the APD via Ca-dependent inactivation (CDI) of I_{CaL}. We call the coupling positive when the sodium-calcium exchanger dominates and negative when the I_{CaL} dominates (46). The coupled system of voltage and Ca cycling can be unstable when the coupling is positive, and vice versa (46). This implies that transient instability of intracellular Ca cycling can promote APD alternans further when the coupling is positive. On the other hand, APD alternans can be reduced when the coupling is negative.

Ca overload also promotes spontaneous Ca release from the SR, as well as formation of Ca waves, which can also cause EADs. However, Ca waves are spatial phenomena and they merit further investigation.

Indeed, the generalization and model reduction limits inclusion of Ca cycling, but we know that Ca effects can contribute to actual EADs (as described in our recent article (24)). To include the intracellular Ca cycling, several variables must be added, which increases system dimensionality and makes analysis much more complex. However, we can analyze CDI as done by Zhao et al. for EADs caused by the transient outward potassium current (I_{to}) (47). In fact, the effect of CDI on EAD generation is similar to that of I_{to} (47).This allows us to investigate the effect of CDI on EAD formation phenomenologically by changing the initial membrane voltage in our simplified model (Fig. S3). One necessary condition for EAD generation shown in our study is that the plateau voltage can enter the basin of EADs, which exists only in an appropriate voltage range. Therefore, we can expect that if voltage early in the AP plateau is too high (mimicking weak CDI) or too low (mimicking strong CDI), the plateau voltage is more likely to bypass the basin for EADs (Fig. S3, *white curves*). For initial voltage (V_0) with both weak ($V_0 = 30$ mV (Fig. S3, *right*)) and strong CDI ($V_0 = -39$ mV (Fig. S3, *left*)), white curves bypass the red basin of EADs, which are thus avoided.

For gradual application of ISO, theoretically we have many choices, such as sigmoidal, linear, or stepwise. Even for stepwise application, we can change it to make ISO application more gradual. Since the stepwise application showed no arrhythmias, a smaller step size or linear increase would fail to show arrhythmias (Fig. S1). To clearly test whether blunting the mismatch between different targets by gradual application will prevent arrhythmias, we chose relatively large application steps (20% of maximal), and no arrhythmias occurred.

βAR stimulation in vivo always accompanies heart rate (HR) acceleration, which may exacerbate the potentiation for alternans or alleviate the potentiation for EADs. However, both transient alternans (Fig. S5 *a*) and EADs (Fig. 6 *D* in Xie et al. (24)) exist in a range of PCLs rather than a single CL. Therefore, as long as the steady-state HR after βAR stimulation is within the transient alternans (or EAD) regime, we will see transient alternans (or EADs).

Our results underscore that transient dynamics provides valuable information that is lacking in steady-state analysis, and they may explain in part why arrhythmias tend to occur when there is a sudden catecholamine surge, such as during excitement, fright, or sudden exercise.

SUPPORTING MATERIAL

Five figures are available at http://www.biophysj.org/biophysj/supplemental/S0006-3495(14)00084-8.

This work was supported by National Institutes of Health grants R37-HL30077 and R01-HL105242 (D.M.B.), K99-HL111334 (D.S.), R01 HL090880 (L.T.I) and R01HL105242 (L.T.I and D.M.B.).

REFERENCES

1. Myerburg, R. J., A. Interian, Jr., …, A. Castellanos. 1997. Frequency of sudden cardiac death and profiles of risk. *Am. J. Cardiol.* 80 (5B):10F–19F.
2. Qu, Z., and A. Garfinkel. 2004. Nonlinear dynamics of excitation and propagation in cardiac muscle. *In* Cardiac Electrophysiology: From Cell to Bedside, 4th ed.. D. P. Zipes and J. Jalife, editors. Saunders, Philadelphia, pp. 339–348.
3. Sato, D., L.-H. Xie, …, Z. Qu. 2010. Irregularly appearing early afterdepolarizations in cardiac myocytes: random fluctuations or dynamical chaos? *Biophys. J.* 99:765–773.
4. Tran, D. X., D. Sato, …, Z. Qu. 2009. Bifurcation and chaos in a model of cardiac early afterdepolarizations. *Phys. Rev. Lett.* 102:258103.
5. Shimizu, W., and C. Antzelevitch. 1999. Cellular and ionic basis for T-wave alternans under long-QT conditions. *Circulation.* 99:1499–1507.
6. Volders, P. G., M. A. Vos, …, R. Lazzara. 2000. Progress in the understanding of cardiac early afterdepolarizations and torsades de pointes: time to revise current concepts. *Cardiovasc. Res.* 46:376–392.
7. Maruyama, M., S.-F. Lin, …, P.-S. Chen. 2011. Genesis of phase 3 early afterdepolarizations and triggered activity in acquired long-QT syndrome. *Circ Arrhythm Electrophysiol.* 4:103–111.
8. Yan, G.-X., Y. Wu, …, P. R. Kowey. 2001. Phase 2 early afterdepolarization as a trigger of polymorphic ventricular tachycardia in acquired long-QT syndrome : direct evidence from intracellular recordings in the intact left ventricular wall. *Circulation.* 103:2851–2856.
9. Luo, C. H., and Y. Rudy. 1994. A dynamic model of the cardiac ventricular action potential. II. Afterdepolarizations, triggered activity, and potentiation. *Circ. Res.* 74:1097–1113.
10. Clancy, C. E., and Y. Rudy. 1999. Linking a genetic defect to its cellular phenotype in a cardiac arrhythmia. *Nature.* 400:566–569.
11. Sato, D., L.-H. Xie, …, Z. Qu. 2009. Synchronization of chaotic early afterdepolarizations in the genesis of cardiac arrhythmias. *Proc. Natl. Acad. Sci. USA.* 106:2983–2988.
12. Burattini, L., W. Zareba, and A. J. Moss. 1999. Correlation method for detection of transient T-wave alternans in digital Holter ECG recordings. *Ann. Noninvasive Electrocardiol.* 4:416–424.
13. Liu, G.-X., B.-R. Choi, …, G. Koren. 2012. Differential conditions for early after-depolarizations and triggered activity in cardiomyocytes

derived from transgenic LQT1 and LQT2 rabbits. *J. Physiol.* 590: 1171–1180.

14. Schwartz, P. J., S. G. Priori, …, R. Bloise. 2001. Genotype-phenotype correlation in the long-QT syndrome: gene-specific triggers for life-threatening arrhythmias. *Circulation.* 103:89–95.
15. Saucerman, J. J., S. N. Healy, …, A. D. McCulloch. 2004. Proarrhythmic consequences of a KCNQ1 AKAP-binding domain mutation: computational models of whole cells and heterogeneous tissue. *Circ. Res.* 95:1216–1224.
16. Soltis, A. R., and J. J. Saucerman. 2010. Synergy between CaMKII substrates and β-adrenergic signaling in regulation of cardiac myocyte Ca^{2+} handling. *Biophys. J.* 99:2038–2047.
17. Heijman, J., P. G. A. Volders, …, Y. Rudy. 2011. Local control of β-adrenergic stimulation: effects on ventricular myocyte electrophysiology and Ca^{2+}-transient. *J. Mol. Cell. Cardiol.* 50:863–871.
18. Terrenoire, C., C. E. Clancy, …, R. S. Kass. 2005. Autonomic control of cardiac action potentials: role of potassium channel kinetics in response to sympathetic stimulation. *Circ. Res.* 96:e25–e34.
19. Abildskov, J. A. 1976. Adrenergic effects of the QT interval of the electrocardiogram. *Am. Heart J.* 92:210–216.
20. Quadbeck, J., and M. Reiter. 1975. Adrenoceptors in cardiac ventricular muscle and changes in duration of action potential caused by noradrenaline and isoprenaline. *Naunyn Schmiedebergs Arch. Pharmacol.* 288:403–414.
21. Vahedi, F., J. Odenstedt, …, L. Bergfeldt. 2012. Vectorcardiography analysis of the repolarization response to pharmacologically induced autonomic nervous system modulation in healthy subjects. *J. Appl. Physiol.* 113:368–376.
22. Yang, J. H., and J. J. Saucerman. 2012. Phospholemman is a negative feed-forward regulator of Ca^{2+} in β-adrenergic signaling, accelerating β-adrenergic inotropy. *J. Mol. Cell. Cardiol.* 52:1048–1055.
23. Behar, M., N. Hao, …, T. C. Elston. 2007. Mathematical and computational analysis of adaptation via feedback inhibition in signal transduction pathways. *Biophys. J.* 93:806–821.
24. Xie, Y., E. Grandi, …, D. M. Bers. 2013. β-adrenergic stimulation activates early afterdepolarizations transiently via kinetic mismatch of PKA targets. *J. Mol. Cell. Cardiol.* 58:153–161.
25. Echebarria, B., and A. Karma. 2007. Mechanisms for initiation of cardiac discordant alternans. *Eur. Phys. J. Spec. Top.* 146:217–231.
26. Fenton, F., and A. Karma. 1998. Vortex dynamics in three-dimensional continuous myocardium with fiber rotation: filament instability and fibrillation. *Chaos.* 8:20–47.
27. Jin, Y.-T., N. Hasebe, …, K. Kikuchi. 2007. Magnesium attenuates isoproterenol-induced acute cardiac dysfunction and β-adrenergic desensitization. *Am. J. Physiol. Heart Circ. Physiol.* 292:H1593–H1599.
28. Fox, J. J., J. L. McHarg, and R. F. Gilmour, Jr. 2002. Ionic mechanism of electrical alternans. *Am. J. Physiol. Heart Circ. Physiol.* 282:H516–H530.
29. Riccio, M. L., M. L. Koller, and R. F. Gilmour, Jr. 1999. Electrical restitution and spatiotemporal organization during ventricular fibrillation. *Circ. Res.* 84:955–963.
30. Garfinkel, A., Y.-H. Kim, …, P.-S. Chen. 2000. Preventing ventricular fibrillation by flattening cardiac restitution. *Proc. Natl. Acad. Sci. USA.* 97:6061–6066.
31. Taggart, P., P. Sutton, …, J. S. Gill. 2003. Effect of adrenergic stimulation on action potential duration restitution in humans. *Circulation.* 107:285–289.
32. Hao, S. C., D. J. Christini, …, B. B. Lerman. 2004. Effect of β-adrenergic blockade on dynamic electrical restitution in vivo. *Am. J. Physiol. Heart Circ. Physiol.* 287:H390–H394.
33. Jordan, P. N., and D. J. Christini. 2007. Characterizing the contribution of voltage- and calcium-dependent coupling to action potential stability: implications for repolarization alternans. *Am. J. Physiol. Heart Circ. Physiol.* 293:H2109–H2118.
34. Hall, K., D. J. Christini, …, J. Billette. 1997. Dynamic control of cardiac alternans. *Phys. Rev. Lett.* 78:4518–4521.
35. Rappel, W.-J., F. Fenton, and A. Karma. 1999. Spatiotemporal control of wave instabilities in cardiac tissue. *Phys. Rev. Lett.* 83:456–459.
36. Tolkacheva, E. G., D. G. Schaeffer, …, W. Krassowska. 2003. Condition for alternans and stability of the 1:1 response pattern in a "memory" model of paced cardiac dynamics. *Phys. Rev. E Stat. Nonlin. Soft Matter Phys.* 67:031904.
37. Guevara, M., G. Ward, …, L. Glass, 1984. Electrical alternans and period-doubling bifurcations. *Proc. IEEE Conf. Comput. Cardiol. 11th, Salt Lake City.* 167–170.
38. Mahajan, A., Y. Shiferaw, …, J. N. Weiss. 2008. A rabbit ventricular action potential model replicating cardiac dynamics at rapid heart rates. *Biophys. J.* 94:392–410.
39. Nakai, J., B. A. Adams, …, K. G. Beam. 1994. Critical roles of the S3 segment and S3-S4 linker of repeat I in activation of L-type calcium channels. *Proc. Natl. Acad. Sci. USA.* 91:1014–1018.
40. Lu, Z., K. Kamiya, …, I. Kodama. 2001. Density and kinetics of I_{Kr} and I_{Ks} in guinea pig and rabbit ventricular myocytes explain different efficacy of I_{Ks} blockade at high heart rate in guinea pig and rabbit. *Circulation.* 104:951–956.
41. Keener, J., and J. Sneyd. 1998. Mathematical Physiology, 1st ed. Springer-Verlag, New York.
42. Rabinovich, M., R. Huerta, and G. Laurent. 2008. Neuroscience. Transient dynamics for neural processing. *Science.* 321:48–50.
43. Ma, W., A. Trusina, …, C. Tang. 2009. Defining network topologies that can achieve biochemical adaptation. *Cell.* 138:760–773.
44. Weiss, J. N., A. Karma, …, Z. Qu. 2006. From pulsus to pulseless: the saga of cardiac alternans. *Circ. Res.* 98:1244–1253.
45. Xie, L.-H., D. Sato, …, J. N. Weiss. 2008. Intracellular Ca alternans: coordinated regulation by sarcoplasmic reticulum release, uptake, and leak. *Biophys. J.* 95:3100–3110.
46. Sato, D., Y. Shiferaw, …, A. Karma. 2006. Spatially discordant alternans in cardiac tissue: role of calcium cycling. *Circ. Res.* 99:520–527.
47. Zhao, Z., Y. Xie, …, L.-H. Xie. 2012. Role of the transient outward potassium current in the genesis of early afterdepolarizations in cardiac cells. *Cardiovasc. Res.* 95:308–316.